NASA TECHNICAL MEMORANDUM

NASA TM X-73659

NASA TM X-73659

(NASA-TM-X-73659) BURNER RIG ALKALI SALT CORROSION OF SEVERAL HIGH TEMPERATURE ALLOYS (NASA) 20 p HC A02/MF A01 CSCL 11F

N77-33313

Unclas
G3/26 49139

BURNER RIG ALKALI SALT CORROSION OF SEVERAL HIGH TEMPERATURE ALLOYS

by D. Deadmore and C. Lowell
Lewis Research Center
Cleveland, Ohio 44135

TECHNICAL PAPER presented at the
One hundred fifty-first meeting of the
Electrochemical Society, Inc.
Philadelphia, Pennsylvania, May 8-13, 1977

BURNER RIG ALKALI SALT CORROSION OF SEVERAL HIGH TEMPERATURE ALLOYS

by D. Deadmore and C. Lowell

National Aeronautics and Space Administration
Lewis Research Center
Cleveland, Ohio 44135

ABSTRACT

The hot corrosion of five alloys was studied in cyclic tests in a Mach 0.3 burner rig into whose combustion chamber various aqueous salt solutions were injected. Three nickel-base alloys (IN-792, IN-738, and IN-100), a cobalt-base alloy (MM-509), and an iron-base alloy (304 stainless steel) were studied at temperatures of 700°, 800°, 900°, and 1000° C with various salt concentrations and compositions. The relative resistance of the alloys to hot corrosion attack was found to vary with temperature and both concentration and composition of the injected salt solution. Results indicate that the corrosion of these alloys is a function of both the presence of salt condensed as a liquid on the surface and of the composition of the gas phases present.

E-9176

INTRODUCTION

Hot corrosion has been shown to be a major cause of failure in gas turbines used in marine, ground power, and, to a lesser extent, aircraft applications. Hot corrosion is usually defined as the accelerated metal loss observed at intermediate temperatures (near 900° C) resulting from sodium sulfate deposition. The literature of hot corrosion has been reviewed by Stringer (ref. 1) and recently expanded by him (ref. 2). Salt is usually considered to be ingested into the engine with air, especially over water, in the form of sea salt whose major constituent is sodium chloride. The salt reacts with sulfur in the fuel during combustion to form sulfates which deposit in the hot section of the turbine. The sulfate deposit is assumed to flux the protective oxide scales normally found on the metals and results in greatly accelerated metal loss by oxidation and sulfidation.

STAR Category 26

In an effort to understand and estimate the extent of hot corrosion, much testing has been performed and much data accumulated. Furnace testing has been used in an attempt to clarify the mechanisms of hot corrosion (e. g., refs. 3 and 4) and burner rig tests (refs. 5 and 6) have been used to rank alloy resistance to attack under conditions intended to simulate some of the engine environment. While the furnace tests have been relatively successful in elucidating hot corrosion attack mechanisms, burner rig tests to rank alloys have been found wanting. Reproducibility has been good within a given laboratory (ref. 6), but laboratory to laboratory correlation has generally been poor (ref. 7) both in terms of degree of attack and relative rankings of the alloys.

The purpose of this work is to try to evaluate the effects of some of the variables of hot corrosion burner rig testing on the degree of attack for a range of typical alloys. The alloys used in this program were IN-100, a nickel-base alloy with little hot corrosion resistance; two nickel-base alloys reputed to have good hot corrosion resistance, IN-738 and IN-792; a cobalt-base alloy with good hot corrosion resistance, MM-509; and an iron-base alloy, 304 stainless steel. These alloys were tested cyclically in a Mach 0.3 burner rig with salts added in the form of aqueous solutions injected into the combustion chamber. The variables were salt composition, salt concentration, and temperature of the alloys tested. The post test evaluation of the alloys consisted primarily of metal thickness loss determinations and metallography, but these data were supplemented with weight loss data and X-ray diffraction.

MATERIALS AND PROCEDURES

The compositions of the alloys used in this program are shown in table I. All but the 304 stainless have been previously tested in hot corrosion by the authors (ref. 6). The alloy expected to have the greatest resistance to hot corrosion (MM-509) has the highest chromium content (23 wt. %) and the alloy expected to have the least hot corrosion resistance (IN-100) has the least chromium content (10 wt. %). All samples were cast by a commercial vendor to

final shape (fig. 1) and all surfaces grit blasted and cleaned with alcohol. Prior to test each sample was measured at A-A (fig. 1) to determine the initial thickness (t_o, fig. 2). This was done with a bench micrometer to a precision of ±2 micrometers (μm) and weighed to ±0.2 milligram (mg).

The burner rig used for these tests is shown in figure 3 and has been described in references 6 and 8. Briefly the rig is a nominal Mach 0.3 Pratt & Whitney-type fired with A-1 jet fuel whose dissolved sulfur content ranges from 0.02 to 0.05 wt.%. The fuel to air ratio was varied from about 0.030 to 0.055, depending upon the sample temperature desired. The range of the operating conditions of the burner is shown in figure 4. Salt was injected into the combustion chamber as an aqueous solution. Eight samples are rotated rapidly in front of the nozzle and reach the desired temperature in a few minutes. After 1 hour the burner pivots away and is replaced by a forced air cooling nozzle for 3 minutes. This cycle is repeated. Approximately every 15 cycles the samples are removed, weighed, and replaced. After 100 cycles the samples are removed, weighed, washed, and reweighed. Washing consisted of immersion of each blade in 300 cc of water at 80° C followed by soft brushing in running water, an alcohol rinse, and air drying. The samples were then cut at A-A (fig. 1), which is the center of the hot zone and where all temperature measurements were made during the run. The cut sections were mounted, metallographically polished, and etched. Thickness measurements were made to determine the final thickness at maximum penetration (t_f) and to calculate metal loss (Δt) as shown in figure 2. While both the initial and final thickness were measured to ±2 μm, experience has shown (ref. 9) that the resultant Δt is only accurate to ±20 μm.

The run conditions are detailed in table II. The oxidation runs (1 and 2) were made to provide baseline Δt measurements for each alloy. Runs 3 to 6 attempted to determine the effect of salt concentration using synthetic sea salt, the most commonly used burner rig corrodent, (see table III for its composition). The largest constituent in sea salt is sodium chloride (NaCl). For runs

7 to 10, it was the only salt used to simplify the temperature variable tests. Runs 11 to 16 were used to investigate the effects of individual salts on hot corrosion and to determine, if possible, the influence of chlorine.

The conditions starred in table II were used for a series of runs in which NiCrAlY coated alloys, highly resistant to hot corrosion, were exposed isothermally for 20 hours to collect for study the deposits formed. After exposure the deposits were scraped and analyzed by X-ray diffraction. After scraping, any remaining deposit was removed by washing (see above). No attack of the NiCrAlY coatings was detected in any of these tests as determined by a complete absence of weight change.

RESULTS AND DISCUSSION

Sea Salt Concentration

All three of the nickel-base alloys responded to variations in salt concentration in the same way (fig. 5). The metal loss increases with increasing salt concentration to a maximum at 2 ppm Na + K (equivalent to 5 ppm total salt) and then drops slightly in the case of IN-100 and precipitously in the case of IN-792 and IN-738. This behavior is similar to that noted by Santoro in reference 8 on S-57 and also to some of his unpublished work on several other alloys. He has attributed this effect to the deposit building to a thickness which, in effect, begins to act as a protective layer. Some evidence for this can be seen in figure 6 which shows the appearance of IN-792 after 100, 1-hour cycles with increasing salt concentration. Up to 2.0 ppm alkali the deposit is light but the corrosion increases. At 3.00 ppm the deposit is very heavy except for the trailing edge which is slightly hotter than the leading edge. However, washing the bar reveals that corrosion is only present at the hot spot where deposition is least. The microstructures of these bars are shown in figure 7. Note the change in magnification of the oxidation sample and that the 3 ppm sample is taken at the trailing edge where maximum attack occurred. The microstructures reveal the typical type of hot corrosion attack expected for these alloys (ref. 6) complete with depletion zone formation, extensive oxide penetration, and sulfides.

The cobalt-base and iron-base alloys (MM-509 and 304 stainless steel) which formed chromia scales behaved differently than the nickel base alloys. The degree of attack on MM-509 continued to increase with salt concentration to the maximum level used, 3.0 ppm, while the stainless steel had a maximum at 0.3 ppm, a minimum at 2.0 ppm and was increasing again at 3.0. No explanation is offered for this behavior but it may be related to the volatiligy of Cr_2O_3 (ref. 10).

From the standpoint of ranking alloys, these tests are most revealing in that for every salt concentration the ranking of the alloys was different. The only consistent alloy was IN-100, which had the greatest attack of any alloy as long as any salt was present. The most erratic performer was 304 stainless. Another complicating factor was that in the runs made to analyze the deposits from sea salt, none of the phases in the deposits could be determined even though strong, sharp diffraction patterns were obtained. This may in part result from the multiplicity of forms into which Na_2SO_4 (the expected major phase) may crystallize. But it appears more likely from the results obtained from other deposits (see below) that the phases are sulfates with mixed cations for which no standard X-ray diffraction pattern exists.

SODIUM CHLORIDE TEMPERATURE EFFECTS

For the conditions of these tests and all others, thermodynamic calculations of the type used by Kohl, et al. were used to predict the composition of the gases at the calculated adiabatic flame temperature and at the temperature of the samples. These calculations predict, in all cases, that only sulfate can be expected to condense at the sample temperatures. However, there was some concern that the residence time (~2 msec) in the combustor might be too short for sodium sulfate formation to take place. Reference 12 would indicate about 1 percent conversion to sulfate. However, Stearns, et al. (ref. 13) indicate 2 msec is ample for complete conversion. The latter view appears correct from the results of our NaCl deposit collection runs. The deposition phase was

unequivocally determined by X-ray diffraction to be Na_2SO_4 Orthorhombic form III (ref. 14). An additional analysis of the deposit was made by wet chemistry for sodium chloride and 0.02 wt.% was found. While this is a small value, it is well above the limits of detectability of the method, 0.002 wt.%. Thus, while Na_2SO_4, was definitely formed, some chloride was present in the deposit.

For all of the alloys tested except 304 stainless the maximum attack occurred at 900° C as is generally assumed for high velocity tests (ref. 1). It is generally believed that at lower temperatures the deposit is solid Na_2SO_4 (M. P. = 884° C) while at higher temperatures the vapor pressure is too high for condensation to occur. Thus, corrosion is thought to occur at intermediate temperatures where a liquid deposit is present. While in general this view seems to be borne out by our results, we still observe extensive corrosion at 1000° C, where little condensation is expected (fig. 8). The macrophotographs (fig. 9) and microstructures (fig. 10) of IN-792 give further evidence of the attack. As in the sea salt tests, the 304 stainless was the exception in having increasing attack with temperature. Again this is thought to be associated with vaporization of the protective chromia scales.

No evidence was found to support Conde's data (ref. 15) indicating another attack maximum at lower temperatures. At 800° and 700° C, even in the colder portions of the bars, there was no metal loss other than from normal oxidation. As can be seen from the unwashed bar at 700° and 800° C (fig. 9), this is not due to a lack of condensate.

ALKALI SULFATES

This part of the program was aimed at determining the effect of alkali sulfates, especially sodium sulfate, on hot corrosion attack in the absence of vapor species containing chlorine or other potentially harmful elements. In the case of the nickel base alloys the maximum attack came with Na_2SO_4 (see fig. 11). This may be explained by the fact that Li_2SO_4 (B. P. = 860° C) is not expected to condense on the samples while K_2SO_4 (M. P. = 1069° C) probably condenses

as a solid. However, the chromia forming alloys (MM-509 and 304 stainless) did not follow the nickel-base alloy trend and were most severely attacked in the Li_2SO_4 test. This is especially true of the MM-509. Figure 12 presents evidence that the attack of MM-509 in the Li_2SO_4 test is both extensive and very similar to the Na_2SO_4 test.

ALKALI CHLORIDES AND SODIUM CARBONATE

As in the case of the sodium chloride, thermodynamic calculations indicate that only K_2SO_4 should condense when KCl is added to the combustion products. This was confirmed by X-ray diffraction analysis of the deposit. Comparable calculations for the LiCl could not be made due to a lack of thermodynamic data for lithium containing vapor species. However, it seems reasonable to expect that, as with the sodium and potassium, only the sulfate should form. However, Li_2SO_4 was identified by X-ray diffraction analysis of the deposit found in cool regions of the collector bars. Therefore, LiCl is converted in the flame to Li_2SO_4.

Again the nickel base alloys acted similarly. As can be seen in figure 13 and confirmed by the microstructures in figure 14, these alloys were attacked the most in the NaCl tests, followed by KCl and then LiCl tests. Of most interest is that the KCl and NaCl tests were more severe than the K_2SO_4 even though the concentration of the alkali's metal was held constant and only sulfates condensed. We interpret this as an indication that the composition of the vapor strongly influences the extent of hot corrosion. Similarly, the MM-509 and 304 stainless were attacked more in the KCl test than in the K_2SO_4, but the MM-509 attack was decreased in the NaCl test compared to the Na_2SO_4 test. Also, both 304 and MM-509 were more attacked in the LiCl test than in either the Li_2SO_4 test or the other chlorides (see fig. 15).

As in the case of the sulfate tests the relative aggressiveness of the alkali salt was consistent with the melting/boiling points except in the cases of MM-509 and 304 in the LiCl test. In the LiCl tests the chlorine in the vapor resulted in only a slight increase in the attack of 304 stainless and a reduction in the attack on MM-509.

Another test of the importance of vapor species was the run containing Na_2CO_3, again at the 3.0 ppm sodium level. As with the chlorides thermodynamic calculations indicate that only Na_2SO_4 should condense and our X-ray diffraction results confirm that it does. Again, this condensate was form III. Figure 16 plots metal recession for the Na_2CO_3 runs and also replots similar data for the NaCl and Na_2SO_4 runs. The furnace tests run by United Technologies (ref. 16) comparing Na_2CO_3 and Na_2SO_4 indicated that Na_2CO_3 was slightly less aggressive, but in the case of the nickel-base alloys of the present the study opposite was true, especially in the case of IN-792. The microstructures of IN-792 (fig. 17) confirm the metal recession results. While the chloride test results can be rationalized by the presence of chlorine in the vapor (ref. 17), the carbonate test results cannot be easily explained. The calculations give no indication of any vapor species being present which might be suspected of accelerating sulfate corrosion. Perhaps such a species exists but it will probably take an experiment similar to reference 13 to establish its identity.

CONCLUSIONS

On the basis of Mach 0.3 burner rig testing involving variations in temperature, salt concentration, and salt composition, the following conclusions about the hot corrosion resistance of IN-100, IN-792, IN-738, MM-509, and 304 stainless steel may be drawn:

1. The ranking of alloys, as determined by burner rig testing, will vary with concentration of the synthetic sea salt added.

2. At low salt deposition rates hot corrosion increases with salt concentration, but at higher deposition rates the reverse may be true.

3. For NaCl additions no low temperature hot corrosion maximum was observed and the hot corrosion increases with temperature to a maximum at about 900° C.

4. The extent of alkali sulfate hot corrosion appears to be related to the melting/boiling points of the sulfate relative to the test temperature.

5. The composition of the gas phase appears to be as important as the condensed phase in controlling hot corrosion.

REFERENCES

1. J. F. Stringer, MCIC-72-08, Metals and Ceramics Information Center, Battelle Columbus Labs., Oh (1972).
2. J. F. Stringer, AGARDograph-200 Advisory Group for Aerospace Research and Development, Paris (France) (1975).
3. N. S. Bornstein and M. A. DeCrescente, Trans. AIME 245, p. 1947 (1969).
4. J. A. Goebel, E. J. Felten, and F. S. Pettit, in "Proceedings of 1974 Gas Turbine Materials in the Marine Environment Conference," MCIC-75-27, J. W. Fairbanks and I. Macklin, Editors, p. 93, Metals and Ceramics Information Center, Battelle Columbus Labs., Oh (1975).
5. H. von E. Doering and P. Bergman, Mater. Res. Stand., 9, 35 (1969).
6. C. E. Lowell and D. L. Deadmore, NASA Tech. Memo X-73465 (1976).
7. NMAB-260 National Materials Advisory Board, Washington, D. C. (1970).
8. G. S. Santoro, NASA Tech. Note D-8395 (1976).
9. C. A. Barrett, G. J. Santoro, and C. E. Lowell, NASA Tech. Note D-7484 (1973).
10. C. A. Barrett and A. F. Pressler, NASA Tech. Note D-8132 (1976).
11. F. J. Kohl, C. A. Stearns, and G. C. Fryburg, in "Metal-Slag Gas Reactions and Processes," Z. A. Foroulis and W. W. Smetyu, Editors, p. 649, The Electrochem. Soc., Princeton, N. J. (1974).
12. V. I. Hanby, J. Eng. Power 96, 129 (1974).
13. C. A. Stearns, et al., NASA Tech. Memo X-73600 (1977).
14. H. Fishmeister, Acta Crystallogr. 7, 776 (1954).
15. A. F. Taylor, et al., "Proceedings of 1976 Gas Turbine Materials in a Marine Environment."
16. N. S. Bornstein and M. A. DeCrescente, Metall. Trans., 2, 2875 (1971).
17. G. C. Fryburg, et al., NASA Tech. Memo X-73599 (1977).

TABLE I. - ALLOY COMPOSITIONS (wt. %)

Element	IN-100	IN-792	IN-738	MM-509	304
Cr	10	12.7	16	23	19
Ni	Bal.	Bal.	Bal.	10	10
Co	15	9.0	8.5	Bal.	-----
Al	5.5	3.2	3.4	----	-----
Ti	4.7	4.2	3.4	.2	-----
Mo	3	2.0	1.75	----	-----
W	-----	3.9	3.9	7	-----
Ta	-----	3.9	.9	3.5	-----
Nb	-----	.9	-----	----	-----
V	1.0	-----	-----	----	-----
Mn	-----	-----	.2	----	2.0
Fe	-----	-----	.5	----	Bal.
Si	-----	-----	.3	----	1.0
Zr	.06	.10	.10	.5	-----
B	.014	.02	.01	----	-----
C	.18	.21	.17	.6	.08

TABLE II. - TEST CONDITION SUMMARY

Run	T, °C	Salt	Concentration, ppm alkali
1	900	None	---
2	1000	None	---
3	900	Synthetic sea salt	0.3
4	↓	↓	1.0
5			2.0
6*			3.0
7	700	NaCl	↓
8	800	↓	
9*	900		
10	1000		
11	900	LiCl	
12*	↓	KCl	
13		Li_2SO_4	
14*		Na_2SO_4	
15		K_2SO_4	
16*		Na_2CO_3	

*Conditions also used for deposition tests.

TABLE III. - SYNTHETIC SEA SALT COMPOSITION

[ASTM D-1141-52 sec. 4.]

Salt	wt. %	Salt	wt. %
NaCl	58.490	$NaHCO_3$	0.477
$MgCl_2 \cdot 6H_2O$	26.460	KBr	.238
Na_2SO_4	9.750	H_3BO_3	.071
$CaCl_2$	2.765	$SrCl_3 \cdot 6H_2O$	.095
KCl	1.645	NaF	.007

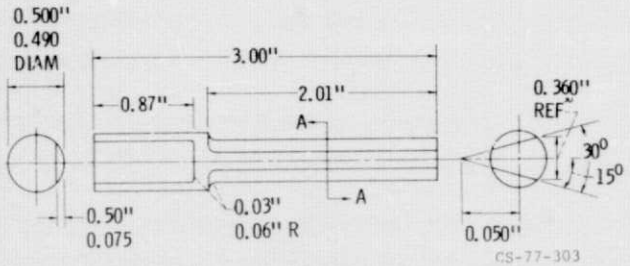

Figure 1. - Burner rig sample geometry.

PLACEMENT OF THICKNESS MEASUREMENTS

$$\Delta t = \frac{1}{2}(t_o - t_f)$$

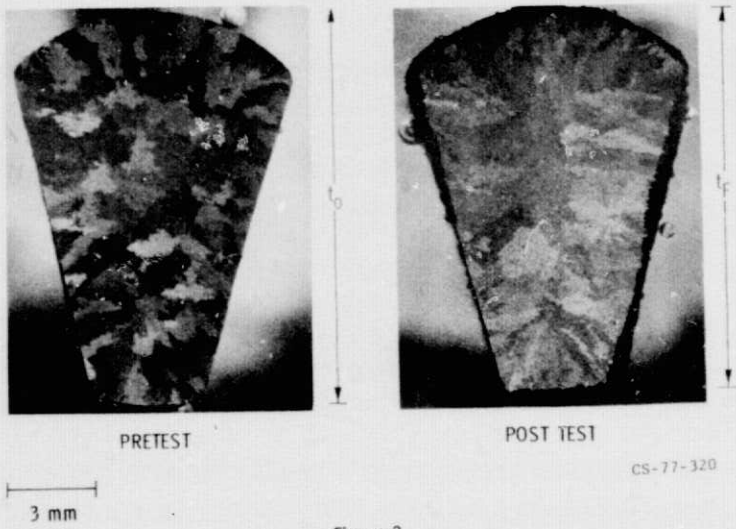

Figure 2.

MACH 0.3 OXIDATION APPARATUS

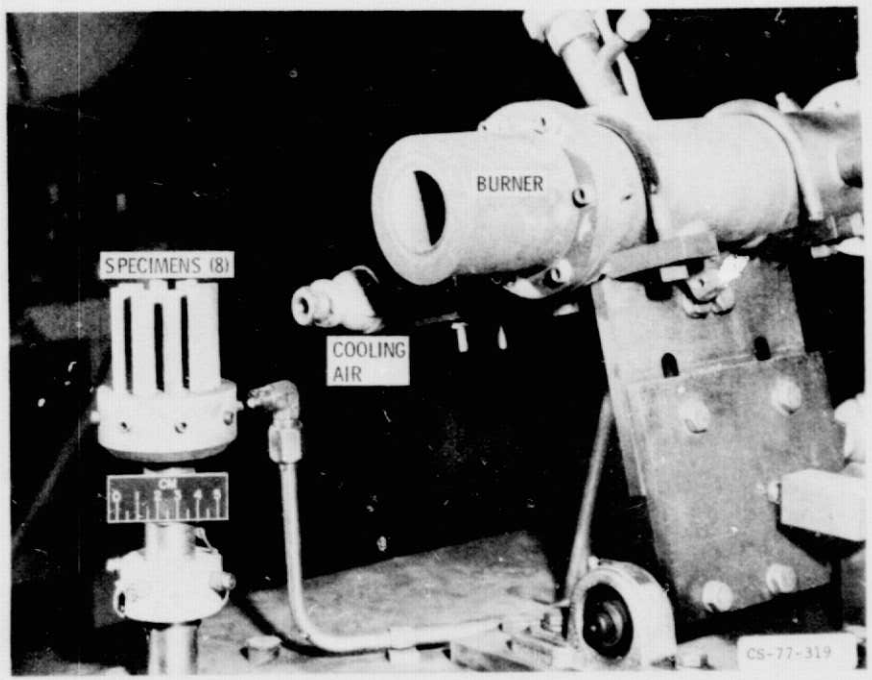

Figure 3.

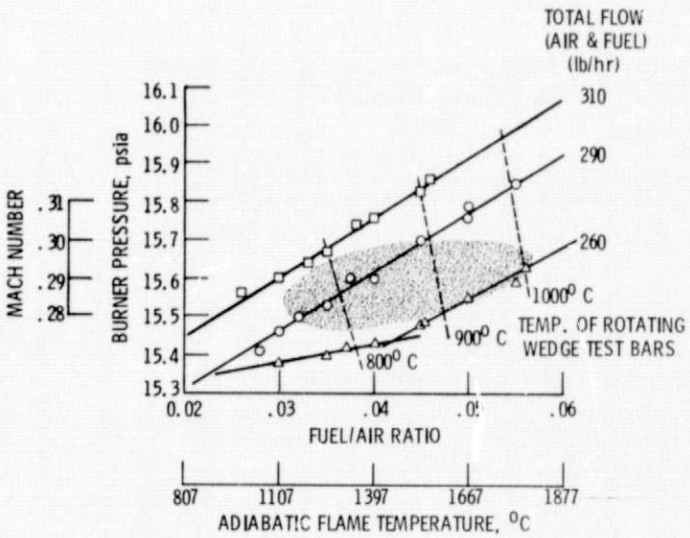

Figure 4. - Burner conditions used for cyclic hot corrosion - 8 rotating wedge bars.

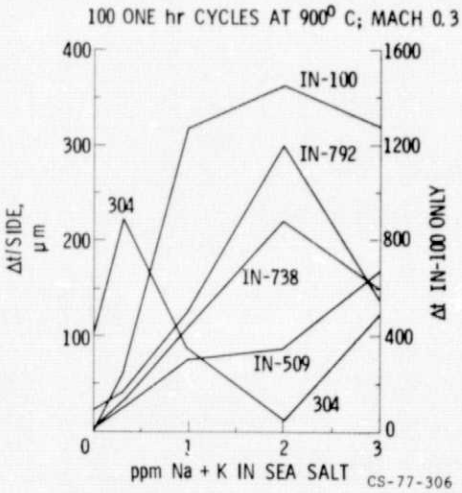

Figure 5. - Effect of synthetic sea salt concentration on hot corrosion.

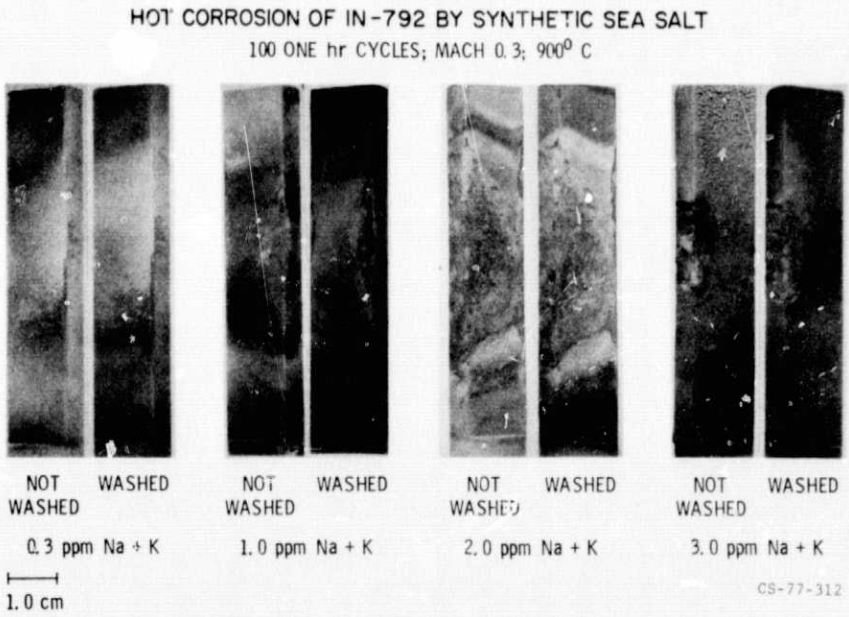

Figure 6.

HOT CORROSION OF IN-792 BY COMBUSTION PRODUCTS
DOPED WITH SYNTHETIC SEA SALT
100 ONE hr CYCLES; MACH 0.3

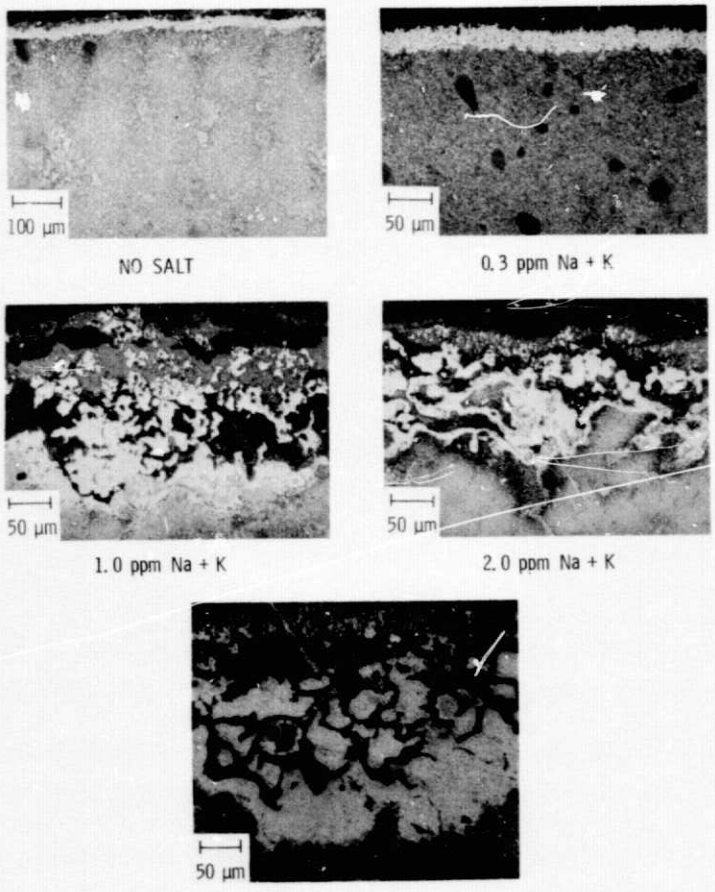

Figure 7.

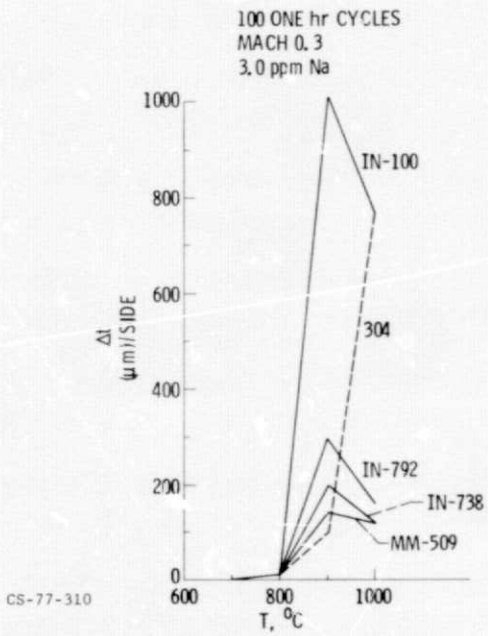

Figure 8. - Effect of temperature on NaCl corrosion.

HOT CORROSION OF IN-792 BY NaCl

100 ONE hr CYCLES: MACH 0.3; 3 ppm Na AS NaCl

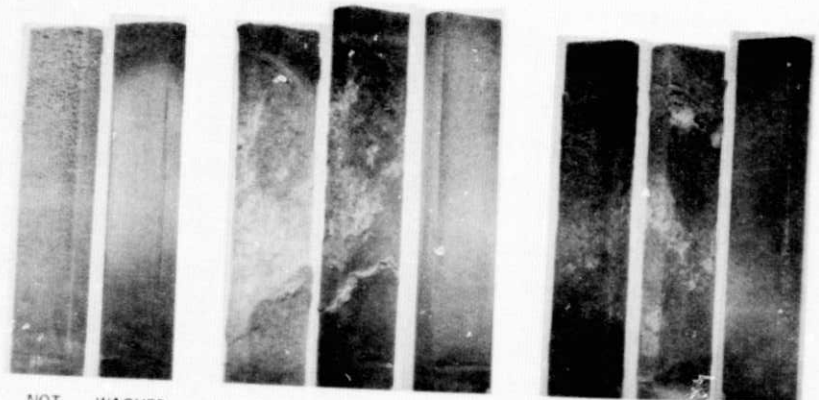

Figure 9.

HOT CORROSION OF IN-792 IN NaCl DOPED COMBUSTION PRODUCTS

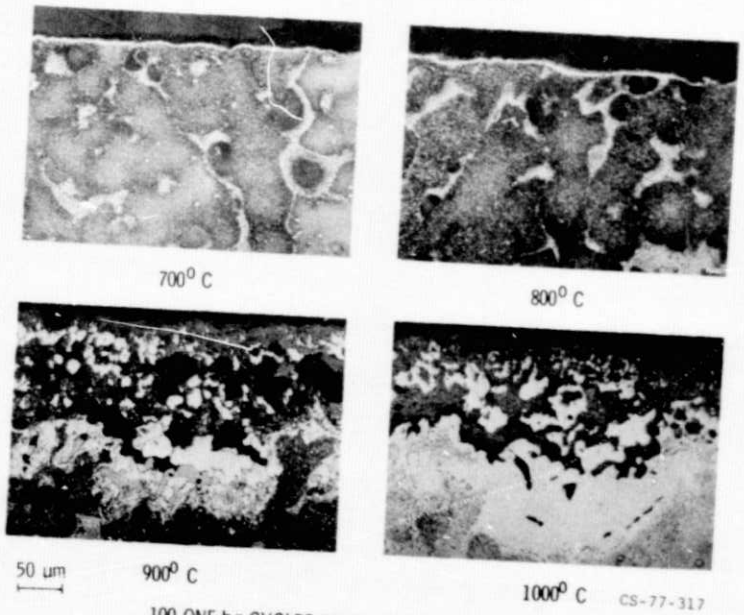

100 ONE hr CYCLES MACH 0.3 3 ppm Na AS NaCl

Figure 10.

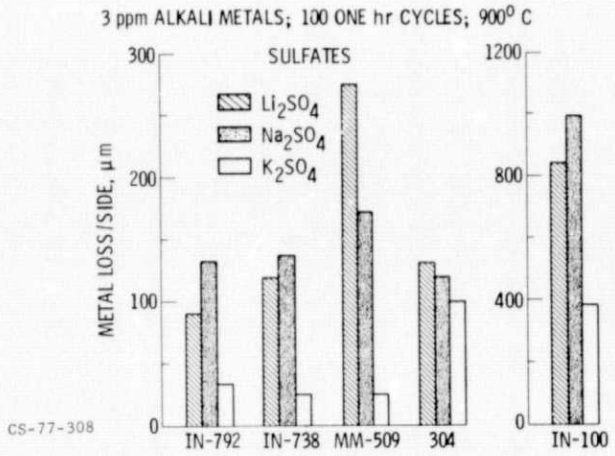

Figure 11. - Metal recession due to addition to alkali sulfates to combustion gases of Mach 0.3 burner rig.

EFFECT OF SULFATE ADDITIONS TO COMBUSTION PRODUCTS ON HOT CORROSION OF MM-509

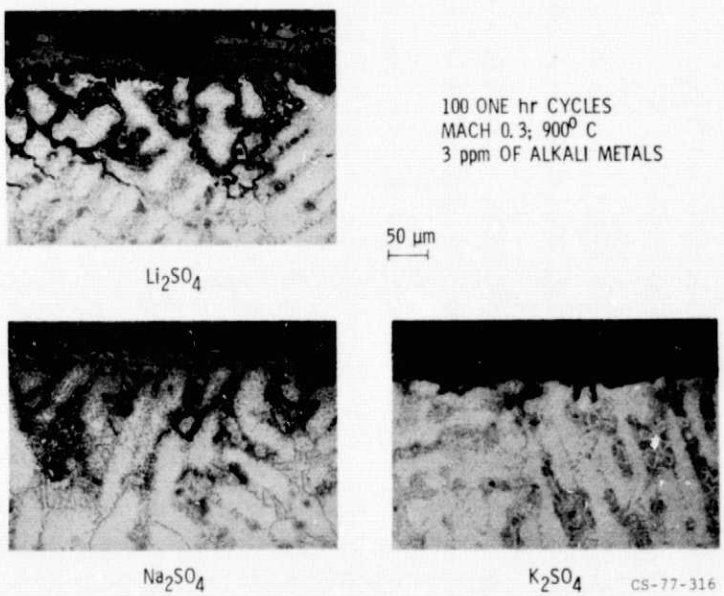

Figure 12.

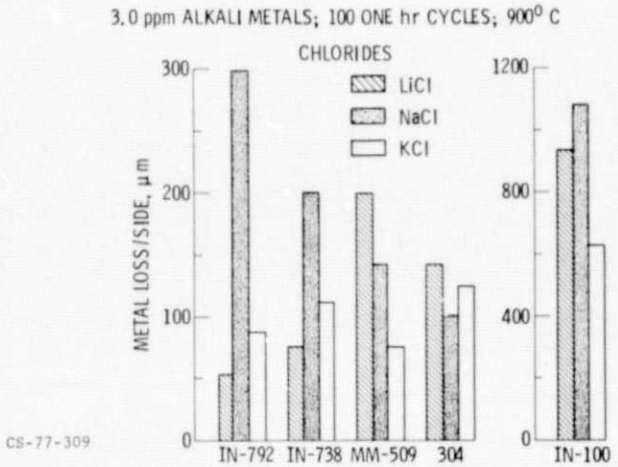

Figure 13. - Metal recession due to addition of alkali chlorides to combustion gases of Mach 0.3 burner rig.

EFFECT OF CHLORIDE ADDITIONS TO COMBUSTION PRODUCTS ON HOT CORROSION OF IN-738

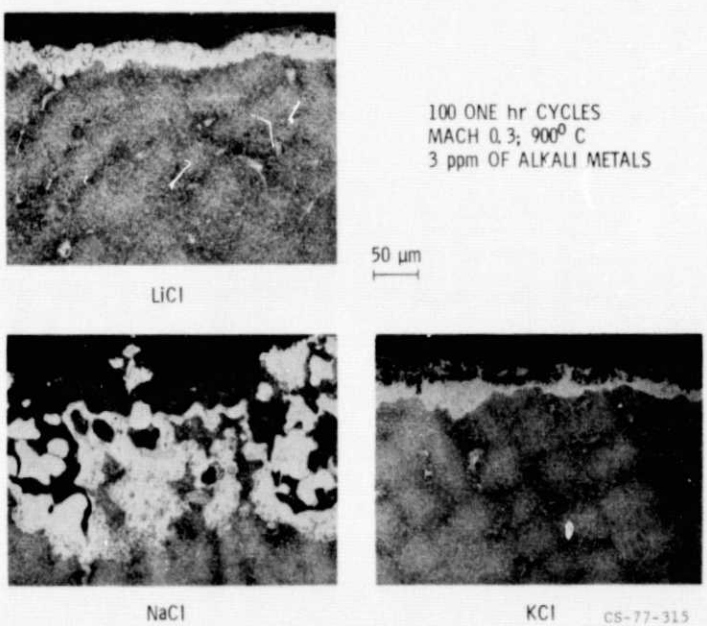

Figure 14.

EFFECT OF CHLORIDE ADDITIONS TO COMBUSTION PRODUCTS ON HOT CORROSION OF MM-509

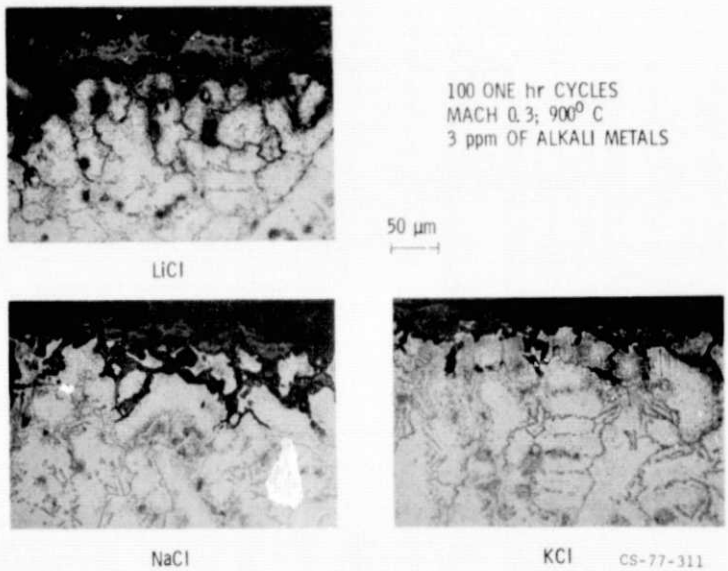

Figure 15.

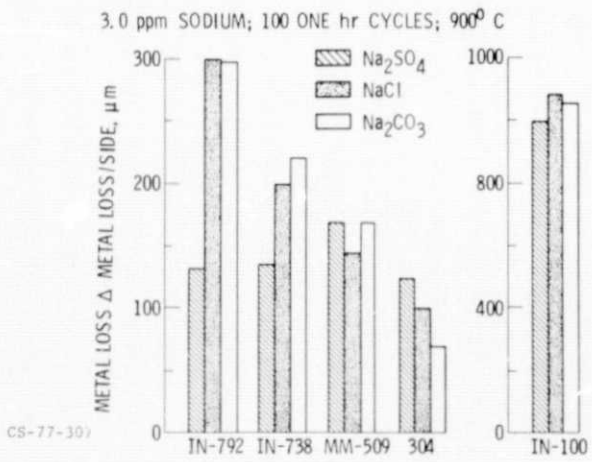

Figure 16. - Metal recession due to addition of sodium salts to combustion gases of Mach 0.3 burner rig.

EFFECT OF SODIUM SALT ADDITIONS TO COMBUSTION PRODUCTS ON HOT CORROSION OF IN-792

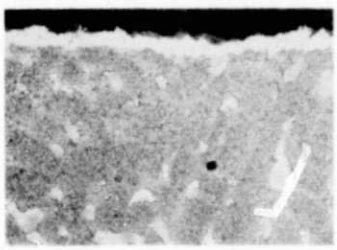

100 ONE hr CYCLES
MACH 0.3; 900° C
3 ppm SODIUM

50 μm

Na_2SO_4

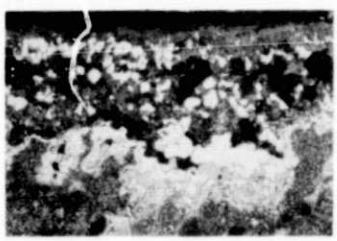

NaCl

50 μm

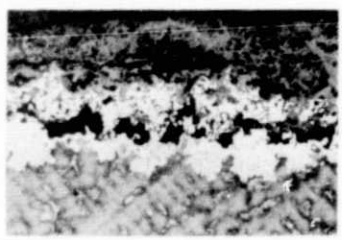

Na_2CO_3

100 μm

GS-77-313

Figure 17.